New constraints on the Neogene exhumation of Bare Mountain, Nevada from apatite fission-track thermochronometry

John A. Stamatakos and David A. Ferrill
Center for Nuclear Waste Regulatory Analyses, Southwest Research Institute,
San Antonio, Texas 78238-5166 (210-522-5247)

Kathy H. Spivey and Alan P. Morris
The University of Texas at San Antonio, San Antonio, Texas

Raymond A. Donelick and Richard A. Ketcham
Donelick Analytical, Katy, Texas

Abstract. Apatite fission track thermochronometry of 33 samples from Bare Mountain and nearby Striped Hills in southwestern Nevada are used to constrain the Neogene exhumation history of the Bare Mountain block. These constraints on the structural evolution of Bare Mountain are critical to tectonic investigations of the potential high-level nuclear waste repository at Yucca Mountain, Nevada. Principally, the results limit the range of admissible tectonic models for Yucca Mountain and provide bounding estimates of the slip-rate of the Bare Mountain Fault. Apatite fission track ages indicate that Bare Mountain was exhumed through the 110 °C isotherm at 14.9 ±3.5 Ma. Exhumation was relatively uniform throughout the mountain except for a possible trend toward less rapid cooling and slightly younger ages at the southern end of the mountain. A 15 Ma exhumation age precludes tectonic models that call upon a shallow regional detachment between Yucca Mountain and the Bullfrog Hills. Stratigraphic and radiometric age data indicate that the Fluorspar Canyon Detachment, which would connect Yucca Mountain to Bullfrog Hills Detachment in such models, was not active until 12 Ma (with Bullfrog Hills Detachment active between 10 and 8 Ma). It seems more likely that Bare Mountain was exhumed by simultaneous motion along a south-southwest directed detachment and the Bare Mountain Fault. In this interpretation, west-dipping dip-slip faults at Yucca Mountain would accommodate hangingwall deformation above the Bare Mountain Fault. If this model is correct, then future motion along Bare Mountain Fault could trigger compensatory slip on faults at Yucca Mountain. Temperature-time models of the distribution of confined track lengths provide estimates of slip rates for the Bare Mountain Fault. A composite temperature-time model for Bare Mountain indicates a slip rate for the Bare Mountain Fault of between 0.01 and 0.44 mm/yr (best-fit of 0.17 mm/yr) based on an average geothermal gradient of 30 °C /km and an average dip of the Bare Mountain Fault of 60°. This range of slip rate estimates is greater than that determined by recent trenching studies in Crater Flat, but significantly less than estimates from recent geodetic studies (level-line survey and GPS measurements). Given the potential effect that future seismicity and fault slip

may have on the safety and performance of a potential repository at Yucca Mountain, we suggest that a slip rate of 0.44 mm/yr represents a reasonably conservative and prudent bounding value for use in future seismic hazard analyses. In contrast to Bare Mountain, two apatite fission track ages from the Striped Hills yield Cretaceous ages. These results indicate significantly different tectonic histories of the two regions at least since the Early Miocene. Previously proposed tectonic models that call on structural correlation of Bare Mountain with the Striped Hills and subsequent offset of ~ 25 km across a right-lateral strike-slip fault are not supported by the new apatite fission track ages.

Introduction

Bare Mountain is a roughly triangular shaped inlier of folded and faulted Proterozoic and Paleozoic meta-sedimentary rocks of the central Basin and Range in southwestern Nevada (Figure 1). It is bound on the east and west by Pliocene to Holocene alluvial valleys and on the north by a thick sequence of Middle to Late Miocene volcanic deposits. Current topographic relief between its highest peaks and the surrounding valleys is approximately one km. Although Bare Mountain lies in the footwall of at least two extensional fault systems and has been referred to as a metamorphic core complex [*Burchfiel et al.*, 1990], it consists predominantly of low-grade metamorphic rocks and lacks a highly mylonitised carapace typical of most core complexes. Its present exposure most likely resulted from tectonic denudation during Basin and Range extension.

The Bare Mountain Fault appears to have played a critical role in the exhumation of Bare Mountain (Figure 1). Because of its proximity to Yucca Mountain and possible influence on the development and current activity of faults within and adjacent to Yucca Mountain, the Bare Mountain Fault is critical to the safety and performance of the proposed high-level nuclear waste repository. The Bare Mountain Fault, which was initially active in the Miocene, continues to be active in the Quaternary, including demonstrable Holocene displacement [*Reheis*, 1988; *Ferrill et al.*, in press]. It has been recognized as the most active fault within 50 km of Yucca Mountain [*Pezzopane*, 1995] and is considered by the *U.S. Department of Energy* [1988] to be a potential source for significant future ground motion in the Yucca Mountain region.

The genetic and kinematic relationships between the Bare Mountain Fault and Yucca Mountain are uncertain. Faults within Yucca Mountain primarily consist of an array of normal or oblique-slip faults that generally dip steeply (70-90°) to the west at the surface [*Scott and Bonk*, 1984]. Their geometry at depth is not well constrained. On the basis of presently available geological data, two end member conceptual models have been proposed to explain the structural configuration of Yucca Mountain in terms of the evolution of the Bare Mountain Fault (Figure 2).

The first model is based on idealized cross sections from *Scott* [1990] and *Hamilton* [1988]. In this model, faults within Yucca Mountain developed in the upper plate of the Fluorspar Canyon Detachment near the detachment's headwall. The subsequent rise of the Bare Mountain block along the Bare Mountain Fault truncated the detachment and isolated the Yucca Mountain faults (Figure 2a). Because of truncation, the model predicts that faults at Yucca Mountain should be largely inactive today.

The proposed detachment in the *Scott* [1990] and *Hamilton* [1988] idealized sections is the contact between the Tertiary volcanics and Paleozoic meta-sedimentary rocks at approximately 2 km depth. Geometric balancing of structural sections across Crater Flat [*Young et al.*, 1993a] require a depth to detachment between 6 and 8 km, possibly between the middle and lower plate (Figure 2a). In this alternative, the detachment does necessarily root to the west of Bare Mountain in the Bullfrog Hills Detachment system [*Young et al.*, 1993b].

The second model is based in part on a schematic cross section of *Gilmore* [1992] and observations noted in *Carr and Monsen* [1988]. In this model, the rise of Bare Mountain was accomplished by coeval motion on a west or southwest directed detachment and the Bare Mountain Fault [*Ferrill et al.*, 1995a]. Accordingly, Yucca Mountain faults developed as

antithetic dip-slip faults in the hangingwall of the Bare Mountain Fault (Figure 2b). Because it remains active, this alternative model predicts that future motion along the Bare Mountain Fault could trigger compensatory deformation within Yucca Mountain. Future deformation at Yucca Mountain is of primary concern because of potential seismic and related damage to mined openings, engineered structures, and radioactive waste packages as well as generation of fracture permeability that could enhance or alter groundwater infiltration and flow.

In this paper, we investigate the tectonic history of Bare Mountain and the related slip history of the Bare Mountain Fault using apatite fission track thermochronometry. For this study we rely on both the distribution of fission-track ages and the temperature-time cooling histories derived from kinetic models of the partial annealing of apatite fission tracks below apatite closure temperature. The first tectonic model, which invokes a regional west-directed shallow detachment between Yucca Mountain and the Bullfrog Hills Detachment to the west is inconsistent with the results of this study. Rather, the Bare Mountain Fault appears to be a dominant structural feature in the Yucca Mountain region from the Middle Miocene to the present. Because of its role in the structural framework of the Yucca Mountain region, slip on the Bare Mountain fault must be carefully considered in analyses of the seismic hazard potential for future slip on Yucca Mountain faults and consequence of faulting on the generation of enhanced pathways for groundwater flow. As we show in this paper, bounding estimates of slip rates for the Bare Mountain Fault over the last five million years from temperature-time cooling histories derived from the fission track data yield values significantly greater than those from fault-trenching studies in Crater Flat [*Klinger and Anderson*, 1994; *Pezzopane*, 1995].

Geologic Framework

Stratigraphy

The geology of Bare Mountain was initially mapped by *Cornwall and Kleinhampl* [1961] at a scale of 1:62,500 and more recently by *Monsen, et al.* [1992] at 1:24,000. Mapping reveals that Bare Mountain consists of a nearly complete 7.5 km thick section of Proterozoic to Mississippian miogeoclinal strata. The section is commonly divided into three tectono-stratigraphic sequences. The lower clastic sequence (Precambrian and Cambrian quartzites and argillites) constitutes the basinward accumulation of continental sediments eroded from an earlier rift-related thermal bulge [*Stewart and Poole*, 1974]. The middle carbonate sequence (Cambrian to Devonian shallow-water deposits) constitutes the carbonate bank developed on the maturing passive margin as the basin was starved of sediment [*Stewart and Poole* 1974]. The upper clastic sequence (Devonian and Mississippian chert pebble conglomerates with detrital carbonates) constitutes flysch deposits shed cratonward into the foredeep ahead of the approaching Roberts Mountain allochthon [*Poole*, 1974].

Except for the intrusion of a small-volume granitic sill in the Cretaceous and several diorite dikes in the Oligocene [*Monsen et al.*, 1992], there was a major hiatus in sedimentation and igneous activity until the Miocene when significant volcanic material (up to 2 km thick) erupted from the Southwestern Nevada Volcanic Field. Maximum eruption rates occurred between 13.3 and 11.5 Ma [*Sawyer et al.*, 1994]. Numerous north-trending quartz-latite dikes also intruded into Bare Mountain during the Miocene [*Carr*, 1984]. One of these dikes at the mouth of Tarantula canyon (Figure 1) yielded a conventional potassium-argon age from mica of 13.9±0.2 Ma [*Monsen et al.*, 1992]. The Miocene volcanics are capped by minor flows of

Late Miocene basalts and Miocene and Pliocene gravels. Pliocene and Quaternary alluvial deposits form aprons on the eastern and southwestern flanks of the mountain.

Metamorphism

Metamorphism of Bare Mountain is dominantly lower and sub-greenschist facies except in the northwest corner where upper greenschist facies rocks with garnet and amphibolite grade rocks with staurolite are present [*Monsen et al.*, 1992]. The age of metamorphism is not entirely known, although the Oligocene diorite dikes cut across metamorphic grade transitions and related ductile structures indicating that metamorphism predates Oligocene dike intrusion (and Miocene extension).

Structure

The structural evolution of Bare Mountain is complex and includes multiple periods of both compressional and extensional deformation. This deformation is manifested by numerous deformational structures including thrust faults and related folds, east-dipping normal faults, detachment faults, and a significant (~40°) structural plunge of the entire Bare mountain block.

Recent zircon fission track results (unpublished data) indicate that contractional faulting along the Meiklejohn Peak and possibly the Panama thrusts (Figure 1) occurred during the Late Carboniferous or Early Permian. Juxtaposition of higher grade over lower grade metamorphic rocks in the northwest corner of Bare Mountain suggests that the Conejo Canyon detachment may have also originated as a thrust fault in the late Paleozoic. Both Conejo Canyon and Meiklejohn Peak thrusts appear to have been reactivated in the Cenozoic as extensional features [*Carr and Monsen*, 1988; *Monsen et al.*, 1992].

Earliest extensional faulting at Bare Mountain appears along a series of normal faults (currently east dipping) that cut the inlier exclusively. These extensional faults together with the earlier contractional structures were rotated to their present orientations by the subsequent tilting (~ 4 ° around a northwest horizonal axis) of the entire Bare Mountain block [*Ferrill et al.*, 1995b]. When the plunge of Bare Mountain is restored, these extensional faults form a listric-fan geometry with significant downward displacement to the southeast. The largest displacement (> 3 km) is along the Gold Ace Mine Fault. The fan appears to project into a southeast directed basal detachment that may now be truncated by the Bare Mountain Fault. The early normal faults are also cut by later detachment faults along the northern and northwestern margins of the mountain; nowhere do they cut Miocene volcanic rocks. These age relationships in concert with paleomagnetic results from Bare Mountain [*Ferrill et al.*, 1995b] suggest growth of this normal fault set and the subsequent tilting of Bare Mountain to the northeast occurred between the latest Eocene and Early Miocene.

The Fluorspar Canyon Detachment which delineates the northern margin of the Bare Mountain block, is a west directed (top to the west) Miocene extensional detachment system. Previous work suggested that this detachment denuded a nearly 2 km thick section of Tertiary volcanic rocks westward off Bare Mountain that led to the subsequent rise of the Bare Mountain block [*Hamilton*, 1988; *Maldonado*, 1990; *Scott*, 1990]. However, as we show here, initial exhumation of Bare Mountain occurs well before the development of the Fluorspar Canyon Detachment. Although the Fluorspar Canyon Fault cannot be mapped continuously to the Bullfrog Hills, it likely connects with the Bullfrog Hills Detachment System to the west [*Hamilton*, 1988; *Maldonado*, 1990; *Scott*, 1990].

The Bare Mountain Fault is an east-dipping normal fault which accommodates up to (and possibly greater than) 3 km of vertical displacement [*Snyder and Carr*, 1984; *Swadely et al.*, 1984; *Reheis* , 1986]. Fault dips mapped at the surface range between 40° and 80° with an average dip of 60° [*Monsen et al.*, 1992]. Stratigraphic evidence indicates activity at least as early as the Middle Miocene. Megabreccias composed of Paleozoic carbonates, presumably derived from an uplifted Bare Mountain block, have been logged in exploratory boreholes in Crater Flat between the 12.7 Ma Tiva Canyon and the 11.6 Ma Rainier Mesa members of the Timber Mountain Tuff [*Carr and Parrish*, 1985; *Faulds et. al.*, 1994]. Similar brecciated Paleozoic strata were also found above 10.5 Ma basalts in the same boreholes and exposed along the southernmost slopes of Bare Mountain [*Swadely and Carr*, 1987]. The Bare Mountain Fault has also been active in the Quaternary (including probable Holocene slip) as indicated by offset alluvial horizons in Crater Flat adjacent to Bare Mountain [*Klinger and Anderson*, 1994; *Reheis*, 1986, 1988] and by systematic differences in alluvial fan development along the eastern and southwestern flanks of the mountain [*Ferrill et al.*, in press].

Sampling and Methodology

Sampling

Thirty-one samples were collected at Bare Mountain (Figure 3, Table 1) from a variety of exposed clastic and igneous rocks including the Precambrian Stirling Quartzite, Precambrian to Cambrian Wood Canyon Formation, Cambrian Zabriskie Quartzite, Ordovician Eureka Quartzite, Mississippian to Devonian Eleana Formation, a Cretaceous granite sill, an Oligocene diorite dike, and several Miocene quartz-latite intrusives. Sample locations were chosen to

provide the maximum spatial and topographic coverage possible. For comparison to the Bare Mountain results, two samples were also collected at the Striped Hills from the Zabriskie Quartzite and Wood Canyon Formation.

Fission Track Age Determinations

Apatite mineral separates, ranging between 70 μm and 300 μm, were obtained from crushed samples using conventional gravimetric and magnetic heavy mineral separation techniques according to procedures outlined in *Crowley et al.* [1989]. Grains were mounted in an epoxy resin on petrographic slides, polished, and etched for 20 (±1) seconds in 5.5 M HNO_3 at 21(±0.5) °C. Each apatite grain mount was then covered by an external fission product detector consisting of a sheet of low uranium muscovite mica. Stacks of up to 20 of these grain mounts were bounded by single chips of CN-1 glass (neutron dosimeter) with their own mica sheets attached. The packages were irradiated at the Texas A&M Nuclear Science Center reactor in position A-2 for 60 minutes at 1 MW power, giving a total thermal neutron fluence of approximately $1x10^6$ neutrons/cm^2. Following irradiation, the micas and glass dosimeters from the sample mounts were etched for 13 minutes in 48 percent HF at 24 °C to reveal induced fission tracks. Dosimeters were calibrated against the Durango standard and ages adjusted using the zeta calibration method [*Naeser and McKee*, 1970; *Hurford and Green*, 1983; *Naeser and Naeser*, 1988]. Natural and induced fission track densities were measured optically (1562.5X magnification) under unpolarized transmitted and reflected light. Fission track lengths were measured in transmitted light (at 1562.5X magnification). The fission track length grain mounts were irradiated with ^{252}Cf fission fragment (Density of ^{252}Cf tracks approximately $5x10^6$ tracks/cm^2) at both ARCO Exploration and Production Technology

(under the direction of S. Bergman) and Rice University (under the direction of R.A. Donelick). Only horizontal confined tracks with well-etched ends were considered as candidates for track-length measurements. Because composition is a critical factor in the kinetics of fission track annealing [e.g. *Green et al.*, 1985], only data from end member fluorapatite grains (which were most common in the Bare Mountain samples) were used in subsequent analyses. Fluorapatite grains, with a closure temperature of 110 °C, were separated from other apatites based on the size of etched figure diameters parallel to the crystallographic c-axis (U.S. Patent Number 5,267,274 to Raymond Donelick). After initial results showed that many samples had low uranium concentrations (less than 4 ppm), ten samples were re-analyzed using approximately three times the original neutron flux ($3x10^6$ neutrons/cm^2) in an attempt to improve sample statistics.

Modeled Temperature-Time Histories

Temperature-time histories were modeled from the apatite fission track ages and the distribution of confined (horizontal) track lengths. These models are based on the observation that fission tracks continue to anneal below closure temperature but at a significantly reduced rate. Because the degree of partial annealing is a function of temperature (resulting in shorter detectable track lengths), the distribution of track lengths provides a sensitive record of thermal history.

Temperature-time models utilize laboratory data from controlled temperature regimes fitted to an empirical equation to predict apatite fission track annealing as a function of time and temperature. The annealing model is based on the Tioga data set of *Donelick and Miller* [1991]. These data were fitted to a fanning Arrhenius equation [*Laslett et al.*, 1987] of the

form employed by *Crowley et al.* [1991]. The initial (unannealed) track length used for fitting was 16.7 μm [*Donelick et al.*, 1990, experiment TI022]. Because the Tioga apatite is more resistant to annealing than the fluorapatite analyzed in this study, a conversion was used based on experiments in which Tioga apatite and end member fluorapatite were annealed side-by-side in the laboratory [*Carlson and Donelick*, unpublished data]. Induced confined (horizontal) fission tracks in the Bare Mountain samples fluorapatites are predicted to average 16.2 μm in length. The resulting model for fluorapatite provides a closer match to the low temperature data presented by *Vrolijk et al.* [1992] than the model of *Laslett et al.* [1987] based on the Durango data set of *Green et al.* [1986]. Prior analyses of some of apatite fission track ages and length distributions for Bare Mountain [*Ferrill et al.*, 1995a; *Spivey et al.*, 1995] were based solely on the *Laslett et al.* [1987] model. New results and re-analyses of previously reported data presented here provide a more accurate fit of the modeled temperature-time histories to the data.

Modeling of the temperature-time histories employed a Monte Carlo approach. In these models, 10,000 possible temperature-time histories were randomly generated with the constraints that they all begin at 25 Ma between 125 and 150 °C, end at the present at 20 °C, and show a progressive decrease in temperature from beginning to end. The underlying assumption is that the samples have only cooled since they passed through the closure temperature. The 25 m.y. time frame was chosen because all samples modeled had fission track ages less than 25 Ma. The 25 m.y. span was separated into 16 individual segments of 1.47 m.y. by 17 nodal points, each allowed to vary randomly within these constraints. A model fission track age and length distribution was calculated for each temperature-time path. The modeled track length population was compared to the track length data using the

Kolmogorov-Smirnov (K-S) statistic [*Press et al.*, 1988], which gives the probability that a random sample taken from the model distribution deviates more from that model distribution than the actual data (defined by the measured track length distribution). A similar statistical parameter that defines the age goodness-of-fit was used to compare the modeled age to the measured age. It assumes that the pooled age (Poisson) and standard deviation from the sample measurement define a Gaussian distribution, in which case the goodness of fit is the proportion of the Gaussian curve which is further away from the pooled age than the model age. Temperature-time histories were judged "acceptable" if both statistics were greater than 0.05. A value of 0.5 for the K-S statistic is expected for samples from the same distribution and thus is the limit of statistical precision. Modeling results were presented by showing the area of temperature-time space that subtends all acceptable histories along with the single best-fit model of the 10,000 randomly-generated cooling curves.

Results

Fission Track Ages

Apatite fission track ages were obtained from 33 samples — 31 from Bare Mountain and 2 from the Striped Hills (Table 1). Most samples yielded reliable results, typified by repeatable ages between initial and subsequent analyses (e.g. sample BMN-10) and a tight cluster of apparent grain ages around their respective means. However, in samples with few apatite grains or low uranium concentration, we noted substantial variability among grain ages (e.g. sample BMW-2). As a result, only samples with at least seven apatite grains and uranium concentrations greater than or equal to 15 ppm were considered reliable. In addition,

we rejected samples in which the mean and pooled ages were significantly different (e.g. Samples BMN-2 and BMW-13 in which the pooled and mean ages do not overlap) because this might signify contamination or a bias in grain selection.

Based on this filter, we deemed ages from 22 of the original 33 samples reliable. Except for the Miocene quartz latite dikes, all ages are significantly younger than the host rocks and thus can be interpreted in the context of the tectonic events discussed above. The three samples from quartz latite dikes (BMN-16, BME-2, and BME-6) agreed (within analytical precision) with the age of 13.9±0.2 Ma K-Ar age of Tarantula Canyon dike [*Monsen et al.*, 1992]. Apatite fission tracks from the other samples at Bare Mountain yielded Miocene ages ranging from 9.2 to 22.7 Ma (Table 1 and Figure 3). The distribution of ages cluster tightly around a mean age of 14.7 ±3.4 Ma (Figure 4). In contrast to Bare Mountain ages, the two fission track ages from the Striped Hills yielded Cretaceous ages of 65.6 and 75.6 Ma (Table 1), suggesting a significantly different tectonic history.

In general, there is little spatial variability in the fission track ages. Fission track ages from Bare Mountain do not vary as a function of elevation (Figure 5a) although a pronounced elevation effect is not necessarily expected in this case because of the limited relief (~1000 m), especially if we assume exhumation rates [*Foster et al.*, 1993] and geothermal gradients [*Sass et al.*, 1994] consistent with those for the Basin and Range from the Miocene to the present. On the basis of these observations, fission track ages for Bare Mountain can be interpreted without regard for sample elevation.

In addition to elevation, apatite fission track ages appear to be independent of geographical position across Bare Mountain from east to west (Figure 5b). However, there is a suggestion that ages decrease slightly from north to south along the eastern face of the mountain (Figure

5c). This correlation is only significant at 90 percent confidence level (r=0.549, for 8 degrees of freedom) and thus should be viewed with caution until more data become available.

Track Lengths

In comparison to expected 16.2 μm fission track length, natural confined track lengths in the Bare Mountain samples ranged between 12.5 and 14.0 μm with average standard deviation (1σ) about the mean lengths of 2.7 μm (Table 1). Relatively long mean track lengths suggest rapid cooling of the samples as they passed through closure temperature. Within Bare Mountain, track length does not vary strongly as a function of fission track age (Figure 6a). However, mean values for a subset of the data from the northwestern third of the mountain (defined in Figure 3) are slightly longer than those from either the northeastern or southern portions of the mountain (Figure 6a). This difference may indicate slightly more rapid cooling (more rapid exhumation) of the northwestern corner of the mountain. The mean track lengths for samples from the Striped Hills are shorter (~11 μm) than the Bare Mountain samples, reflecting both older age and perhaps a less rapid cooling history.

Temperature-Time Analysis

Cooling histories from temperature-time analyses were determined for the Bare Mountain samples based on fission-track ages and distributions of the lengths of confined fission tracks (Figure 7). For these analyses, only samples with at least 20 confined tracks that passed our criteria for reliable fission track ages (Table 1) were modeled using the Monte Carlo approach outlined above. Based on this filter, we obtained temperature-time histories for 10 samples (Table 1, Figure 8).

The best-fit curves for these 10 cooling histories show relatively rapid initial cooling, within the first 5 Ma after the samples passed through the 110 °C closure temperature, followed by significantly slower cooling at temperatures below 50 °C. In several samples a second period of rapid cooling within the last 5 Ma is also evident (e.g. samples BMW-12A, BME-18, and BMN-1). The most tightly constrained cooling curves are from the northwest corner of the mountain in samples with a large number (> 50) of confined tracks.

Composite cooling curves (average of best-fit and upper and lower acceptable limits) were constructed by averaging nine of the ten cooling histories (Figure 9). Because its fission track age corresponds to the age of dike intrusion [*Monsen et al.*, 1992], the cooling history of sample BME-2 (from the Tarantula Canyon dike) may reflect dike emplacement rather than exhumation. Averaging of the other nine cooling histories is valid here because the age data indicate that all samples share a common thermal history that reflects tectonic processes significantly younger than the depositional ages of the host rocks. From these composite curves, we have estimated throw-rates and slip-rates for the Bare Mountain Fault for three 5–m.y. periods (Table 2). These rates assume an average geothermal gradient for the Basin and Range of 30°C/km [*Sass et al.*, 1994]. Slip-rates were determined for the average 60° dip on the Bare Mountain Fault assuming only dip-slip motion. Lower geothermal gradients, that may have existed in the Basin and Range prior to crustal extension [*Fitzgerald et al.*, 1991], or higher geothermal gradients, that may have existed during the development of the Southwestern Nevada Volcanic Field, would result in appropriately higher or lower throw and slip rates.

Discussion

Exhumation History

Apatite fission track ages indicate cooling of currently exposed rocks on Bare Mountain through fluorapatite closure temperature (110 °C) at about 14 or 15 Ma. Ages distributed around the mountain are similar suggesting uniform exhumation, at least after passing through the 110 °C isotherm, except for the possibility of slightly younger fission track ages on the southern end of the mountain. The relatively long track lengths (Figure 6) and initially rapid cooling curves in the temperature-time models (Figure 8) indicate rapid exhumation at first followed by reduced exhumation to the present. Interestingly, the 15 Ma exhumation age predates the main eruptive phase of the Southwestern Nevada Volcanic Field [*Sawyer et al.*, 1994], suggesting that Miocene volcanism may be a consequence of—but clearly did not initiate—detachment faulting at Bare Mountain.

On the basis of the fission track ages and modeled temperature histories reported here, we propose the following tectonic history for Bare Mountain since the beginning of the Neogene (Figure 10).

(1) Prior to 15 Ma Bare Mountain consisted of Paleozoic (or possibly Mesozoic) thrusts and folds dissected by a series of southeast-dipping normal faults (the listric fan). Before 15 Ma Bare Mountain was tilted approximately 40° to the northeast about a northwest-southeast horizontal axis.

(2) Between 14 and 15 Ma, rocks at the current surface of Bare Mountain were exhumed through 110 °C by a combination of detachment faulting along the mountain's southwestern margin and normal faulting (the Bare Mountain Fault) along its eastern margin. Contrary to previous interpretations [*Hamilton*, 1988; *Maldonado*, 1990; *Scott*, 1990], our results indicate that the Fluorspar Canyon Detachment did not initiate exhumation. Where it is mapped, the Fluorspar Canyon Detachment cuts the Miocene volcanics [*Monsen et al.*, 1992]. Development of an angular unconformity in the volcanic sections north and northwest of Bare Mountain suggests initial motion at about 12 Ma [*Ferrill et al.*, 1995]. Radiometric ages from *Maldonado* [1990] indicate that the upper plate of the Bullfrog Hills Detachment, of which the Fluorspar Canyon was a part, was not active until between 10 and 8 Ma.

A more likely explanation for the exhumation of Bare Mountain is that the 15 Ma uplift represents the last stage of unroofing along a southwest directed detachment. This detachment could also explain the development of the 40° northeast structural plunge of the mountain. In this interpretation, Bare Mountain first rolled to the northeast (sometime between the Eocene and Early Miocene) in response to unroofing on a southwest-directed detachment, akin to differential motion observed further west in the Funeral Mountains [*Hoisch and Simpson*, 1993]. Once rocks at the present exposure surface were above the 110 °C isotherm, exhumation was more uniform, although the possible north-to-south decrease in fission track ages suggests that minor differential tilting may have continued into the Middle Miocene.

We also envision contemporaneous motion along the Bare Mountain Fault because exhumation seems to be relatively uniform especially across the mountain from west to

east. The brecciated carbonates within the Miocene volcanic strata of Crater Flat [*Carr and Parrish*, 1985] indicate motion since at least 11.5 Ma. Moreover, no Miocene volcanics are mapped on Bare Mountain south of the Fluorspar Canyon Detachment, suggesting that Bare Mountain may have been a significant topographic feature during the main pulse of Middle Miocene volcanism. This interpretation is consistent with generalized isopach maps of the Miocene volcanics presented in *Byers et al.* [1976]. Detailed determinations of isopach thicknesses of the Miocene volcanics in the Amargosa Desert on the lee side of Bare Mountain would offer definitive proof of Bare Mountain's topography in the Miocene and allow exhumation rates to be interpreted in terms of uplift [*England and Molnar*, 1990].

(3) From 13.5 to 10.0 Ma Miocene volcanics erupted from the Southwestern Nevada Volcanic Field and were deposited around Bare Mountain. Bare Mountain continued to be exposed and the Bare Mountain Fault remained active, as indicated by brecciated carbonates derived from Bare Mountain intercalated with Miocene volcanics in Crater Flat.

(4) After about 12 Ma the Fluorspar Canyon Detachment was active, creating the distended volcanic deposits north and northwest of Bare Mountain. The Bare Mountain Fault remains active, with differential Holocene slip along the fault (increasing to the south).

Because of the 15 Ma age of the Bare Mountain Fault and timing of Bare Mountain exhumation, the array of steeply-dipping faults at Yucca Mountain could not have developed in the headwall of a regional, west directed detachment as proposed by *Scott* [1990] and

Hamilton [1988] (Figure 2a). Rather, fission track ages from Bare Mountain support the alternative model (Figure 2b) in which faults at Yucca Mountain developed to accommodate hangingwall deformation above the Bare Mountain Fault. This implies that as long as the Bare Mountain Fault remains active, compensatory activity along the Yucca Mountain faults seems likely. This possible link between the Bare Mountain Fault and Yucca Mountain faulting must be carefully considered in evaluations of the potential seismic risks for the proposed high-level nuclear waste repository at Yucca Mountain.

Correlation with the Striped Hills

The Cretaceous fission track ages from the Striped Hills indicate a significantly different tectonic history than that at Bare Mountain, at least since the Neogene. Based on simplified structural relationships like fold vergence and bedding dip, *Caskey and Schweikert* [1992] proposed that the Panama and Meiklejohn Peak thrusts, as part of the Sevier fold and thrust belt, should be correlated with the east- and west-vergent CP and Belted Range thrusts respectively. From this reconstruction, *Caskey and Schweikert* [1992] interpreted up to 30 km of right-lateral slip between Bare Mountain and the Striped Hills, along the hypothetical Stewart Valley-State Line Fault.

This interpretation was challenged by *Snow* [1992] who considers the Meiklejohn Peak and Panama thrusts on Bare Mountain to be Permian structures of the Last Chance Allochthon. *Snow* [1994] also argues that sedimentary facies of many of the Lower Paleozoic units between Bare Mountain and the Striped Hills are too different to allow restoration in the manner proposed by *Caskey and Schweikert* [1992].

Although the fission track results presented here do not necessarily rule out the *Caskey and Schweikert* 's [1992] reconstruction, differences in ages between Bare Mountain and the Striped Hills suggest that the two ranges were isolated from one another at least since the Early Miocene. Therefore, even if Bare Mountain and the Striped Hills were at one time connected, their separation by the proposed Stewart Valley-State Line Fault must have occurred prior to the Early Miocene and prior to the initiation of the Bare Mountain Fault. Consequences of this hypothetical strike-slip faulting would not bear on the Neogene tectonic evolution of Bare Mountain.

Constraints on the Seismic Hazard Assessment at Yucca Mountain

Although there is evidence for Quaternary slip on splays of the Bare Mountain Fault exposed in alluvium, there is little agreement on the amount or timing of this slip [*Swadley et al.*, 1984; *Reheis*, 1986; 1988; *Klinger and Anderson*, 1994]. Throw rates (the authors did not incorporate fault dip into their calculations) from these trenching studies range between 0.01 and 0.19 mm/yr [*Pezzopane*, 1995]. Estimates of the age of latest fault motion range from 9,000 to over 100,000 years ago. It is important to note that all estimates of throw (slip) rate and timing from these trenching studies are based on single rupture surfaces.

In contrast, relative uplift rates from geodetic measurements are significantly greater than the trenching studies. Level-line surveys between Tonopah and Las Vegas, Nevada in 1907, 1915, and 1984 indicate a slip rate of approximately 1.6 mm/yr for the Bare Mountain Fault [*Gilmore*, 1992]. Recent Global Position System (GPS) measurements also indicate relative uplift rates for Bare Mountain greater than 1.0 mm/yr [*Ferrill et al.*, 1995a].

The temperature-time analyses indicate a slip rate for the Bare Mountain Fault of between 0.01 and 0.44 mm/yr (Table 2). Unlike single-event readings from trenching studies and the relatively small time frame of the geodetic measurements, estimates from fission tracks represent an integrated slip-rate over the past 5 m.y. Given the potential effect that future seismicity and fault slip may play on the safety and performance of a potential repository at Yucca Mountain, we suggest that a slip rate of 0.44 mm/yr represents a reasonably conservative and prudent bounding value for future seismic hazard analyses. However, observation of recent strain from geodetic measurements must also be evaluated, given the possibility that these data reflect a recent acceleration of slip along the Bare Mountain Fault. More importantly, the large difference in slip-rates from the various techniques (or even the same technique in the case of the fault-trenching studies), indicates that multiple techniques need to be employed in order to obtain accurate assessments of the potential hazards associated with fault slip in and around Bare Mountain.

Conclusions

Apatite fission track ages from Bare Mountain, Nevada indicate exhumation and possibly uplift of Bare Mountain as early as 15 Ma. Exhumation appears to be related to coeval motion along a southwest directed detachment and the Bare Mountain Fault. Because Bare Mountain was exhumed prior to the development of the Fluorspar Canyon detachment, tectonic models that call on a regional west-directed shallow detachment between Yucca Mountain and the Bullfrog Hills Detachment to the west, are unrealistic. Rather, the Bare Mountain Fault

appears to be a dominant structural feature in the Yucca Mountain Region from the Middle Miocene to the present.

Temperature-time analyses of the distributions of fission track lengths indicate an integrated slip rate for the Bare Mountain Fault of between 0.01 and 0.44 mm/yr. These values are greater than those estimated from trenching studies in Crater Flat but less than those derived from recent geodetic studies.

Apatite fission track ages from the Striped Hills indicate cooling through 110 °C during the Cretaceous. The contrast between Cretaceous exhumation of the Striped Hills and Miocene exhumation of Bare Mountain suggests that rocks of the two ranges have been structurally separated since at least the Early Miocene. Palinspastic reconstructions that indicate separation of the Striped Hills from Bare Mountain by up to 30 km of right-lateral motion along the hypothetical Stewart Valley-State Line Fault are not supported by these results.

Acknowledgments. This paper was prepared as a result of work performed by the Center for Nuclear Waste Regulatory Analyses (CNWRA) for the Nuclear Regulatory Commission (NRC) under contract number NRC-02-93-005. The activities reported here were initiated on behalf of the NRC Office of Nuclear Regulatory Research and continued on the behalf of the Office of Nuclear Material Safety and Safeguards. This paper is an independent product of CNWRA and does not necessarily reflect the views or regulatory position of the NRC. We thank Steve Young, Sid Jones, Ronald Martin, Gerry Stirewalt, Esther Cantu and Larry McKague for assistance in sampling and manuscript preparation. We appreciate editorial comment by Barbara Long, and technical comments by Mike Conway and Wesley C. Patrick.

We also thank Mark Cloos for providing the Durango age standard, Jan Schreurs for providing the CN-1 dosimeter, and Steve Burgman for help with the early ^{252}Cf irradiations.

References

Burchfiel, B.C., D.S. Cowen, and G.A. Davis, Tectonic overview of the Cordilleran orogen in the western United States, *in* The Cordilleran Orogen: Conterminous U.S., edited by B.C. Burchfiel, P.W., Lipman, and M.L. Zoback, *The Geology of North America G-3*, Geological Society of America, Boulder, Colorado, 407-479, 1992.

Byers, F.M. Jr., W.J. Carr, P.P. Orkild, W.D. Quinlivan, and K.A. Sargent, Volcanic suites and related cauldrons of Timber Mountain-Oasis Valley Caldera Complex, Southern Nevada, *Geological Survey Professional Paper 919,* U.S. Geological Survey, Washington DC, 70 pp., 1976.

Carr, M.D., and S.A. Monsen, A Field Trip Guide to the Geology of Bare Mountain, edited by D.L. Weide and L.L. Faber, *Special Publication of the Geoscience Department, University of Nevada at Las Vegas*, Las Vagas, Nevada, pp. 50–57, 1988.

Carr, W.J., Regional structural setting of Yucca Mountain, southwestern Nevada, and late Cenozoic rates of tectonic activity in part of the southwestern Great Basin, Nevada and California, *U.S. Geological Survey Open-File Report 84-854*, 109 pp., 1984.

Carr, W.J. and L.D. Parrish, Geology of drill hole USW-VH-2 and structure of Crater Flat, southwestern, Nevada, *U.S. Geological Survey Open-File Report 85-475*, 41 pp., 1985.

Caskey, S.J., and R. Schweikert, Mesozoic deformation in the Nevada Test Site and vicinity: Implications for the structural framework of the Cordilleran fold and thrust belt and Tertiary extension north of Las Vegas Valley, *Tectonics, 11*, 1214–1331, 1992.

Cornwall H.R., and F.J. Kleinhampl, Geology of the Bare Mountain Quandrangle, *U.S. Geological Survey Geological Quadrangle Map GQ-157*, scale 1:62,500, 1961.

Crowley, K.D., C.W. Naeser, and N.D. Naeser, Fission Track Analysis: Theory and Applications, Short Course Manual, Geological Society of America Annual Meeting, St. Louis, Missouri, Geological Society of America, 269pp., 1989.

Donelick R.A., M.K. Roden, J.D. Mooers, B.S. Carpenter, and D.S. Miller, Etchable length reduction of induced fission tracks in apatite at room temperature (~23 °C): Crystallographic orientation effects and "initial" mean lengths, *Nuclear Tracks and Radiation Measurements*, *17*, 261–265, 1990.

Donelick, R.A., and D.S. Miller, Enhanced TINT fission track densities in low spontaneous track density apatites using 252Cf-derived fission fragment tracks: A model and experimental observations, *Nuclear Tracks and Radiation Measurements*, *18*, 301–307, 1991.

England, P., and P. Molnar, Surface uplift, uplift of rocks, and exhumation of rocks, *Geology*, *19*, 1173–1177, 1990.

Faulds, J.E., J.W. Bell, D.L. Feuerbach, and A.R. Ramelli, Geologic map of the Crater Flat Area, Nevada, *Nevada Bureau of Mines and Geology Map 101*, scale 1:24,000, 1994.

Ferrill, D.A., J.A. Stamatakos, S.M. Jones, B. Rahe, H.L. McKague, R.H. Martin, and A.P. Morris, Quaternary slip history of the Bare Mountain Fault (Nevada) from the morphology and distribution of alluvial fan deposits, *Geology*, in press, 1996.

Ferrill, D.A., G.L. Stirewalt, D.B. Henderson, J.A. Stamatakos, A.P. Morris, B.P. Wernicke, and K.H. Spivey, *Faulting in the Yucca Mountain region: Critical review and analyses of tectonic data from the Central Basin and Range*, CNWRA 95-017, Center for Nuclear Waste Regulatory Analyses, San Antonio, Texas, 1995a.

Ferrill, D.A., D.B. Henderson, J.A. Stamatakos, K.H. Spivey, and A.P. Morris, Tectonic processes in the central Basin and Range, *NRC High-Level Radioactive Waste Research at CNWRA, January–June 1995, CNWRA 95-01S*, edited by B. Sagar, Center for Nuclear Waste Regulatory Analyses, San Antonio, Texas, 6.1–6.27, 1995b.

Fitzgerald, P.G., J.E. Fryxell, and B.P. Wernicke, Miocene crustal extension and uplift in southeastern Nevada: Constraints from fission track analysis, *Geology, 19*, 1013–1016, 1991.

Frizzel, V.A. and J. Shulters, Geologic map of the Nevada Test Site, southern Nevada, *U.S. Geological Survey Miscellaneous Investigations Series Map I-2046*, Scale 1:100,000, 1990.

Foster, D.A., A.J. Gleadow, S.J. Reynolds, and P.G. Fitzgerald, Denudation of metamorphic core complexes and the reconstruction of the transition zone, west central Arizona: Constraints from apatite fission track thermochronology, *Journal of Geophysical Research, 98(B2)*, 2167-2185, 1993.

Green, P.F., I.R. Duddy, A.J.W. Gleadow, and P.R. Tingate, Fission track annealing in apatite: Track length measurements and the form of the Arrhenius plot, *Nuclear Tracks and Radiation Measurements, 10*, 323-328, 1985.

Green, P.F., I.R. Duddy, A.J.W. Gleadow, P.R. Tingate, and G.M. Laslett, Thermal annealing of fission tracks in apatite 1: Qualitative description, *Chemical Geology, 59*, 237–253, 1986.

Gilmore, T.D., Geodetic leveling data used to define historical height changes between Tonopah Junction and Las Vegas, Nevada, *U.S. Geological Survey Open File Report 92-450*, 16 pp., 1992.

Hamilton, W.B., Detachment faulting in the Death Valley region, California and Nevada, *in* Geologic and Hydrologic Investigations of a Potential Nuclear Waste Disposal Site at Yucca Mountain, Southern Nevada:, edited by M.D. Carr and J.C. Yount, *U.S. Geological Survey Bulletin 1790*, 51–85, 1988.

Hoisch T.D., and C. Simpson, Rise and tilt of metamorphic rocks in the lower plate of a detachment fault in the Funeral Mountains, Death Valley, California, *Journal of Geophysical Research, 98*, 6805–6827, 1993.

Hurford, A.J., and P.F. Green, The zeta calibration of fission track dating, *Isotope Geosciences*, 1, 285-317, 1983.

Klinger, R.E., and L.W. Anderson, Topographic profiles and their implications for late Quaternary activity of the Bare Mountain Fault, Nye County, Nevada, *Geological Society of America Abstracts with Program—1994 Annual Meeting*, Seattle, Washington, Geological Society of America, *26(2)*, 63, 1994.

Laslett, G.M., P.F. Green, I.R. Duddy, and A.J.W. Gleadow, Thermal annealing of apatite fission tracks in apatite 2: A quantitative analysis, *Chemical Geology, 65*, 1–13, 1987.

Maldonado, F., Structural geology of the upper plate of the Bullfrog Hills detachment fault system, southern Nevada, *Geological Society of America Bulletin, 102*, 992–1006, 1990.

Monsen, S.A., M.D. Carr, M.C. Reheis, and P.A. Orkild, Geologic map of Bare Mountain, Nye County, Nevada, *U.S. Geological Survey Miscellaneous Investigations Series Map I-2201*, scale 1:24,000, 1992.

Naeser C.W., and E.H. McKee, Fission track and K-Ar ages from Tertiary ash-flow tuffs, north-central Nevada, *Geological Society of America Bulletin, 81*, 3375–3384, 1970.

Naeser C.W., and N.D. Naeser, Fission-track dating of Quaternary events, *Geological Society of America Special Paper 227*, 1988.

Pezzopane, S.K., Preliminary Table of Characteristics of Known and Suspected Quaternary Faults in the Yucca Mountain Region, *U.S. Geological Survey Administrative Report*, U.S. Geological Survey, Reston, VA, 1995.

Poole, F.G., Flysch deposits in the Antler foreland basin, western United States, *in* Tectonics and Sedimentation, edited by W.R. Dickenson, *Society of Economic Paleontologists and Mineralogists Special Publication 22*, 58–82, 1974.

Press, W.H., B.P. Flannery, S.A. Teukolsky, and W.T. Vetterling, Numerical Recipes in C, Cambridge University Press, Cambrdige England, 735 pp., 1988.

Reheis, M.C., Preliminary study of Quaternary faulting on the east side of Bare Mountain, Nye County, Nevada, *in* Geologic and Hydrologic Investigations of Yucca Mountain, Nevada, *U.S. Geological Survey Open-File Report 85-576*, 103-111, 1986.

Reheis, M.C., Preliminary study of Quaternary faulting on the east side of Bare Mountain, Nye County, Nevada, *in* Geologic and Hydrologic Investigations of a Potential Nuclear Waste Disposal Site at Yucca Mountain, Southern Nevada, edited by M.D. Carr and J.C. Yount, *U.S. Geological Survey Bulletin 1790*, 103–112, 1988.

Sass, J.H., A.H. Lachenbruch, S.P. Galanis Jr., P. Morgan, S.S. Priest, T.H. Moses Jr., and R.J. Munroe, Thermal regime of the southern Basin and Range Province: Heat flow data from Arizona and the Mojave Desert of California and Nevada, *Journal of Geophysical Research*, 99 *(B11)*, 22093–22229, 1994.

Sawyer, D., R.J. Fleck, M.A. Lanphere, R.G. Warren, D.E. Broxton, and M. Hudson, Episodic caldera volcanism in the Miocene southwestern Nevada volcanic field: Revised stratigraphic framework, $^{40}Ar/^{39}Ar$ geochronology and implications for magmatism and extension, *Geological Society of America Bulletin, 106*, 1304–1318, 1994.

Scott, R.B., Tectonic setting of Yucca Mountain, southwest Nevada, *in* Basin and Range Extensional Tectonics Near the Latitude of Las Vegas, Nevada, edited by B.P. Wernicke, *Geological Society of America Memoir 176*, 251–282, 1990.

Scott, R.B., and J. Bonk, Preliminary geologic map of Yucca Mountain, Nye County, Nevada with geologic sections, 1:12,000, U.S. *Geological Survey Open-File Report 84-494*, 1984.

Snow, J.K., Large-magnitude Permian shortening and continental-margin tectonics in the southern Cordillera, *Geological Society of America Bulletin, 104*, 80–105, 1992.

Snow, J.K., Mass Balance of Basin and Range extension as a tool for geothermal exploration, *Geothermal Resource Council Transactions, 18*, 23–30, 1994.

Snyder, D.B., and W.J. Carr, Interpretation of gravity data in a complex volcano-tectonic setting, southwestern Nevada, *Journal of Geophysical Research, 89*, 10193–10206, 1984.

Spivey, K.H., D.A. Ferrill, J.A. Stamatakos, A.P. Morris, R.A. Donelick, and S.R. Young, Uplift and cooling history of Bare Mountain, Nevada, from apatite fission track thermochronology, *Geological Society of America Abstracts with Program—1995 Annual Meeting*, New Orleans, Louisiana, Geological Society of America, *27*, A-389, 1995.

Stewart, J.H., and F.G. Poole, Lower Paleozoic and uppermost Precambrian Cordilleran miogeosyncline, Great Basin, western United States, *in* Tectonics and Sedimentation, edited by W.R. Dickenson, *Society of Economic Paleontologists and Mineralogists Special Publication 22*, 28–57, 1974.

Swadley, W.C., D.L. Hoover, and J.N. Rosholt, Preliminary report on Late Cenozoic faulting and stratigraphy in the vicinity of Yucca Mountain, Nye County, Nevada, U.S. *Geological Survey Open-File Report 84-788*, 42 pp., 1984.

Swadley, W.C., and W.J. Carr, Geologic map of the Quaternary and Tertiary deposits of the Big Dune Quadrangle, Nye County, Nevada, and Inyo County, California, *U.S. Geological Survey Miscellaneous Investigations Series Map I-1767*, scale 1:48,000, 1987.

U.S. Department of Energy, *Site Characterization Plan: Yucca Mountain Site, Nevada Research and Development Area,* DOE/RW-0199, U.S. Department of Energy, Office of Civilian Radioactive Waste Management, Washington DC, 1988.

Vrolijk, P., R.A. Donelick, J. Queng, and M. Cloos, Testing models of fission track annealing in apatite in a simple thermal setting: Site 800, Leg 129, *Proceedings of the Ocean Drilling Program Scientific Results, 129*, 169–176, 1992.

Young, S.R., A.P. Morris, and G.L. Stirewalt, Geometric analyses of alternative models of faulting at Yucca Mountain, Nevada, *Proceedings of the Third Annual International High-Level Radioactive Waste Management Conference, Las Vegas, Nevada, American Nuclear Society, La Grange Park, Illinois, 2*, 1818–1825, 1993a.

Young, S.R., G.L. Stirewalt, and A.P. Morris, *Geometric Models of Faulting at Yucca Mountain*, CNWRA 92-008, Center for Nuclear Waste Regulatory Analyses, San Antonio, Texas, 1993b.

Figure Captions

Figure 1. Simplified geologic map of Yucca Mountain region after *Frizzel and Shulters* [1990] and *Monsen et al.* [1992]. Sample locations at Bare Mountain and the Striped Hills for apatite fission track thermochronometry are shown.

Figure 2. Stylized end member conceptual tectonic models of Bare Mountain and Crater Flat as proposed by (a) *Scott* [1990] and *Hamilton* [1988], and (b) *Ferrill et al.* [1995a].

Figure 3. Map of Bare Mountain showing fission track age results. Sample identifications in gray denote samples that failed minimum acceptable criteria. Samples with an * are mean ages, all others are pooled ages. Reference datum and coordinate axes used to construct graphs in Figure 5 are also shown. Dashed lines mark geographic division between domains used in Figure 6.

Figure 4. Histogram showing distribution of apatite fission track ages for Bare Mountain. Mean for all samples and mean for all samples* that exclude two oldest ages (> 20 Ma) are shown.

Figure 5. (a) Fission track age plotted as a function of sample elevation for Bare Mountain samples. Error bars are $\pm$ 1 σ. Expected relationship between age and elevation for three different cooling rates are also shown. (b) Apatite fission track age

plotted as a function of east-west distance across Bare Mountain measured from the reference datum defined in Figure 3. Dashed line shows the average across the profile. (c) Apatite fission track age plotted as a function of north-south distance across Bare Mountain measured from reference datum defined in Figure 3. The correlation coefficient for the least-squares linear regression is r.

Figure 6. (a) Track lengths plotted as a function of fission track age. Mean values for the three regions (northeast, northwest, and south) defined in Figure 3 are also shown. Error bars are 1σ around mean values. (b) Similar plot to (a) with the addition of the two Striped Hills samples.

Figure 7. Histograms showing distribution of confined track lengths for 10 samples used in temperature-time analyses.

Figure 8. Temperature-time cooling curves of Bare Mountain samples modeled from distribution of confined fission track lengths. Solid curve is best-fit curve. Dashed lines show upper and lower acceptable limits given by Kolmogorov-Smirnov statistic and age goodness of fit statistics.

Figure 9. Composite temperature-time cooling models based on 9 of the 10 curves shown in Figure 8 (BME-2 not used because it was from Miocene dike). Shaded region is 1σ around the average curves. Solid curve is average of sample best-fit curves. Dashed curves are means of the lower and upper acceptable bounds.

Figure 10. Schematic diagram illustrating tectonic evolution of Bare Mountain from Middle Miocene to present based on structural/stratigraphic relationships and apatite fission track results.

Table 1. Fission Track Results from Bare Mountain and Striped Hills, Nevada

Site	Rock Type	Elev (m)	ρ_s	N_s	ρ_i	N_i	ρ_d	N_d	N_g	Q	χ^2	Pooled Age	Mean Age	N_t	Length μm	S.D. μm	U_c
BFH-1[d]	CZw (schist)	988	0.168	157	3.616	3386	5.052	4220	40	0.371	P	13.9±1.2	16.3±1.7	75	14.3±0.2	1.61	45
BFH-2[d]	CZw (schist)	1073	0.170	159	3.993	3739	5.055	4220	34	0.181	P	12.8±1.1	16.3±2.3	101	14.1±0.2	1.66	59
BFH-3[d]	Zs (quartzite D)	1091	0.209	124	4.561	2712	5.058	4220	26	0.156	P	13.7±1.3	16.9±1.8	51	13.8±0.3	1.92	48
BMN-1[b]	Kg (granite)	1110	0.033	17	0.733	374	4.088	4088	34	0.716	P	11.0±2.8	9.6±2.8	26	13.9±0.2	0.96	8
BMN-1[a, d]	Kg (granite)	1110	0.029	21	2.282	1636	13.84	4380	39	0.891	P	10.6±2.3	8.8±2.5	51	14.1±0.2	1.04	8
BMN-2[c]	Td (diorite)	1061	0.148	13	2.292	201	5.070	4220	11	0.188	P	19.5±5.6	34.7±15.5	20	13.8±0.5	1.75	15
BMN-4	Cz (quartzite)	1360	0.227	82	3.933	1163	5.073	4220	23	0.023	F	21.2±2.5	22.7±3.5	4	12.4±1.8	3.05	48
BMN-5	Cz (quartzite)	1232	0.149	75	3.232	1624	5.075	4220	22	0.204	P	13.9±1.7	17.7±4.1	14	13.4±0.5	1.81	29
BMN-10	Cz (quartzite)	1677	0.152	22	5.524	799	5.078	4220	14	0.008	F	8.3±1.8	8.5±3.0	5	12.4±2.6	5.10	66
BMN-10[a]	Cz (quartzite)	1677	0.195	50	15.04	3859	14.19	4380	24	0240	P	10.9±1.6	10.0±2.5	14	12.5±1.1	4.10	53
BMN-13	Oe (quartzite)	1787	0.148	46	3.321	1033	5.084	4220	12	0.116	P	13.5±2.1	13.1±3.7	12	13.4±0.9	2.31	49
BMN-15	Cz (quartzite)	1610	0.313	11	5.201	749	5.087	4220	11	0.007	F	18.1±2.9	15.2±6.3	0			48
BMN-15[a,b]	Cz (quartzite)	1610	0.078	5	4.641	297	14.26	4380	5	0.533	P	14.3±6.4	16.0±9.1	4	14.5±0.3	0.54	15
BMN-16	Tl(latite)	1133	0.052	27	0.087	455	4.699	4086	36	0.337	P	16.6±3.3	16.6±4.8		n.m.		19
BMN-19	Cz (quartzite)	1055	0.103	28	1.592	431	5.090	4220	24	0.311	P	19.6±3.9	23.6±5.9	33	13.4±0.4	2.03	15
BMN-19[a,d]	Cz (quartzite)	1055	0.090	26	6.545	1871	14.32	4380	32	0.005	F	11.8±2.4	18.3±6.6	76	13.6±0.2	1.93	21
BMN-20[b]	Oe (quartzite)	1445	0.142	4	1.136	32	3.957	4045	4	0.772	P	29.3±15.6	39.7±15.7	12	14.5±1.3	1.29	17
BMN-21[b]	Oe (quartzite)	1330	0.108	2	3.071	57	5.084	4119	2	0.850	P	10.6±7.6	5.4±7.6	0			21
BME-1	MDe (congl)	1317	0.183	42	3.954	906	5.061	4220	20	0.541	P	13.9±2.2	12.0±3.1	12	13.9±0.5	1.47	49
BME-2[b]	Tl (latite)	1226	0.062	35	0.807	458	5.064	4220	33	0.899	P	23.0±4.1	24.3±4.6	18	12.5±0.8	3.16	8
BME-2[a, d]	Tl (latite)	1226	0.044	18	2.395	990	14.05	4380	27	0.556	P	15.2±3.6	14.7±4.2	33	13.2±0.5	2.72	8
BME-3[b]	CZw (schist)	1024	0.072	12	1.044	173	5.067	4220	15	0.346	P	20.9±6.3	27.6±14.9	2	8.8±4.5	4.51	9
BME-3[a,b]	CZw (schist)	1024	0.013	3	0.705	166	14.12	4380	19	0.200	P	15.1±8.8	23.8±14.4	11	12.3±0.9	2.72	2
BME-6[b]	Tl (latite)	1660	0.040	6	0.751	113	4.706	4086	5	0.933	P	14.8±6.2	10.2±4.7	84	13.6±0.2	1.89	7
BME-17[b]	Oe (quartzite)	1207	0.008	1	1.047	128	4.990	4119	13	0.763	P	2.3±2.3	1.8±1.8	0			10
BME-17[a, b]	Oe (quartzite)	1207	0.021	1	2.376	111	14.34	4380	7	0.947	P	7.7±7.7	3.0±3.2	0			11
BME-18[d]	Zs (quartzite E)	1189	0.232	87	4.115	1546	5.037	4119	32	0.134	P	16.8±1.9	20.4±3.6	30	13.7±0.4	1.72	46
BMW-1[b]	Zs (schist C)	1128	0.039	18	0.548	254	4.108	4088	24	0.734	P	17.3±4.3	18.1±5.1	8	12.1±1.0	2.76	7
BMW-2[b]	Zs (quartzite D)	976	0.058	25	0.347	149	4.129	4.88	28	0.085	P	41.1±9.0	62.0±17.5	23	12.5±0.7	3.08	4
BMW-2[a,b]	Zs (quartzite D)	976	0.011	2	0.953	166	13.90	4380	11	0.608	P	10.1±7.1	9.9±8.7	33	13.2±0.5	3.02	4
BMW-3[d]	Zs (quartzite D)	997	0.115	89	2.034	1569	4.150	4088	33	0.132	P	14.0±1.6	15.5±3.0	25	13.0±0.4	2.04	28
BMW-5	Cz (quartzite)	1220	0.128	28	1.608	352	4.171	4088	21	0.011	F	19.7±3.9	19.9±8.7	7	12.6±0.7	1.81	18
BMW-5[a]	Cz (quartzite)	1220	0.020	3	3.366	517	13.98	4380	12	0.812	P	4.8±2.8	2.6±1.8		n.m.		12
BMW-6[d]	Zs (quartzite D)	1049	0.137	30	1.892	413	5.093	4220	18	0.833	P	22.0±4.2	28.7±5.9	51	13.2±0.3	1.53	20
BMW-12A[d]	Zs (quartzite D)	1098	0.074	10	1.905	256	5.081	4220	14	0.405	P	11.8±3.8	19.6±6.6	23	13.2±0.7	2.07	18
BMW-12B	Td (diorite)	1098	0.123	12	2.683	261	5.096	4220	7	0.059	P	13.9±4.1	20.3±9.8	0			29
BMW-13[c]	Zs (quartzite A)	939	0.155	28	1.297	234	5.130	4119	9	0.045	F	36.4±7.4	11.9±8.5	5	13.8±1.2	2.35	17
BMW-13[a]	Zs (quartzite A)	939	0.019	2	1.751	186	14.46	4380	8	0.053	P	9.2±6.6	19.7±13.9	12	12.3±0.7	2.24	
BMW-15	Zs (quartzite A)	1103	0.185	13	3.50	252	3.950	4045	7	0.155	P	12.1±3.5	10.4±5.2	0			53
BMW-16[b]	Oe (quartzite)	1785	1.953	15	43.62	335	3.943	4045	2	0.994	P	10.5±2.8	10.5±0.4	0			51
BMW-17	Zs (schist C)	1170	0.111	8	1.493	108	3.935	4.45	8	0.906	P	17.3±6.4	13.9±7.6	0			21
SH-1	Cz (quartzite)	1024	0.615	50	2.178	177	3.928	4045	15	0.236	P	65.6±10.7	62.3±14.3	17	11.0±0.7	2.67	27
SH-2	CZw (schist)	1012	0.513	218	1.628	668	3.921	4045	23	0.827	P	75.6±6.4	77.2±7.9	75	11.3±0.3	2.23	19

Notes: Rock types are defined in *Monsen et al.*, [1992]. ρ_s, ρ_i, and ρ_d are the spontaneous, induced and dosimeter track densities (10^6 tracks/cm^2). N_s, N_i, and N_d are the number of spontaneous, induced and dosimeter fission tracks. N_g is the number of apatite grains. Q is the probability that χ^2 value is greater than reported for a single population of grain ages (for values of Q > 0.05, pooled age is more accurate); pooled age is the fission track age based on sum total of spontaneous and induced tracks for all grains in sample; mean age is arithmetic mean of individual grain ages (errors are 1σ). P is the result χ^2 test (P for pass, F for fail). N_t is the number of horizontal confined tracks measured in track length analyses (errors are 1σ, n.m indicates no measurement). S.D is the standard deviation of the track length distribution. U_c is the concentration of ^{238}U in ppm.

[a] second analyses with approximately 3x initial irradiation.
[b] site that did not pass minimum criteria, $N_g \geq 7$ and $U_c \geq 15$ for initial irradiation and $N_g \geq 7$ and $U_c \geq 5$ for 3x re-irradiation
[c] large discrepancy between pooled and mean age
[d] used for temperature-time analyses

37/48

Table 2. Slip Rates for Bare Mountain Fault from Temperature-Time Analyses

Age Span (Ma)	Lower Limit		Mean of Best-Fit Curves		Upper Limit	
	Throw Rate (mm/yr)	Slip Rate[1] (mm/yr)	Throw Rate (mm/yr)	Slip Rate[1] (mm/yr)	Throw Rate(mm/yr)	Slip Rate[a] (mm/yr)
0-5	0.01	0.01	0.15	0.17	0.38	0.44
5-10	0.06	0.07	0.20	0.24	0.25	0.29
10-15	0.21	0.24	0.29	0.33		

[a] slip rate based on a 60° fault dip

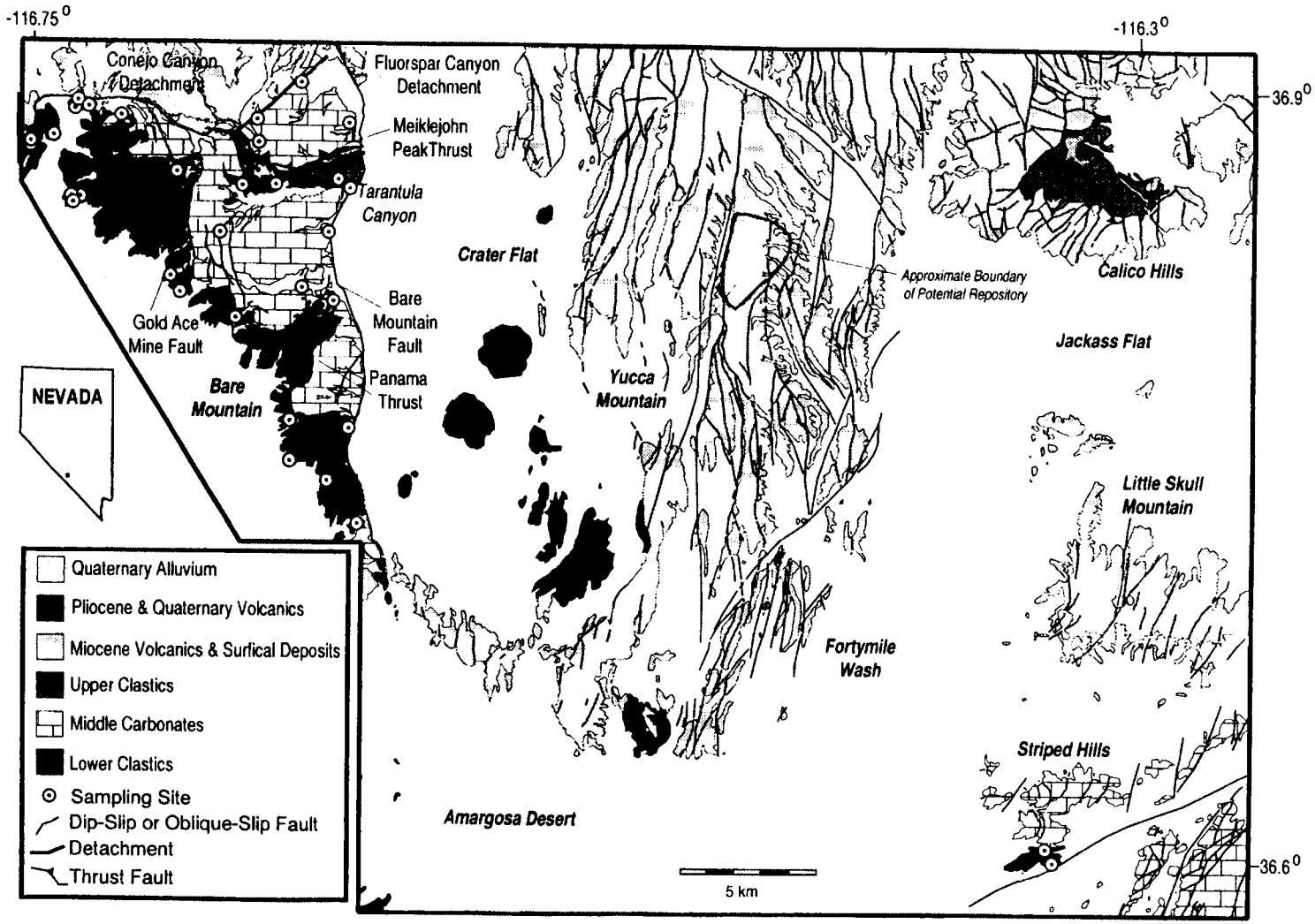

Stamatakos et al. , Figure 1.

39/48

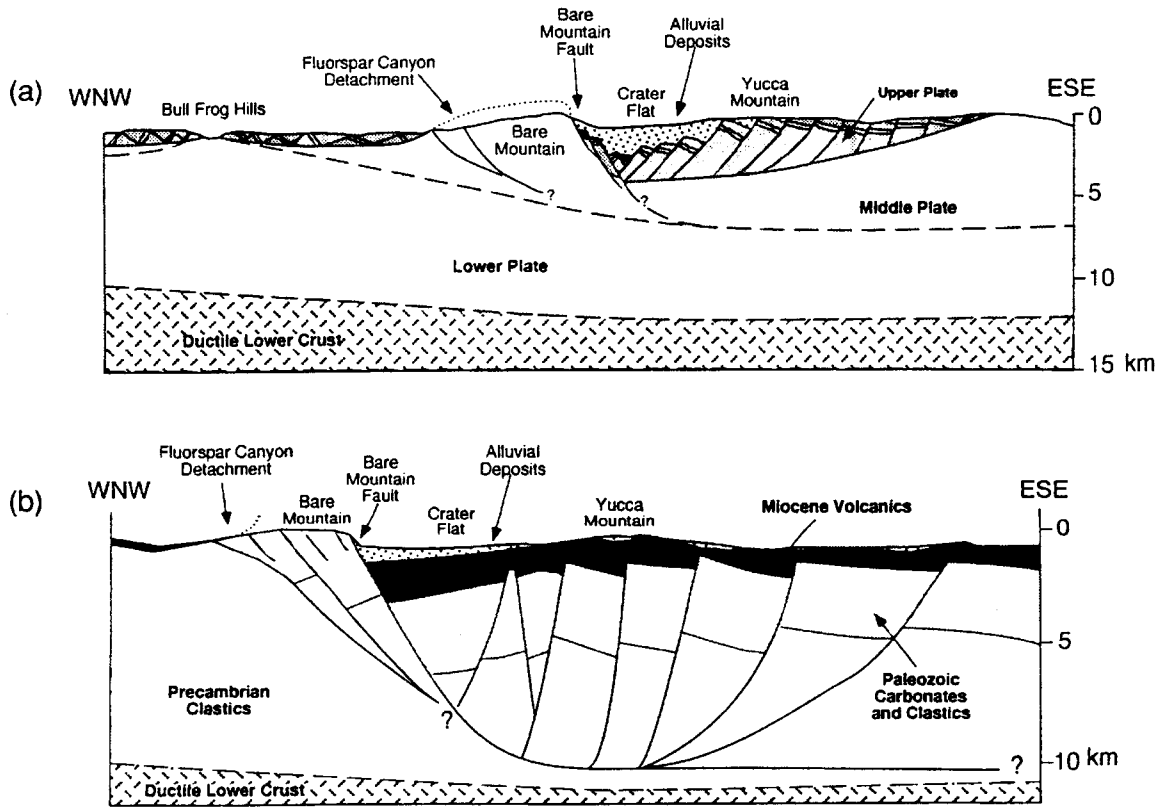

Stamatakos et al., Figure 2.

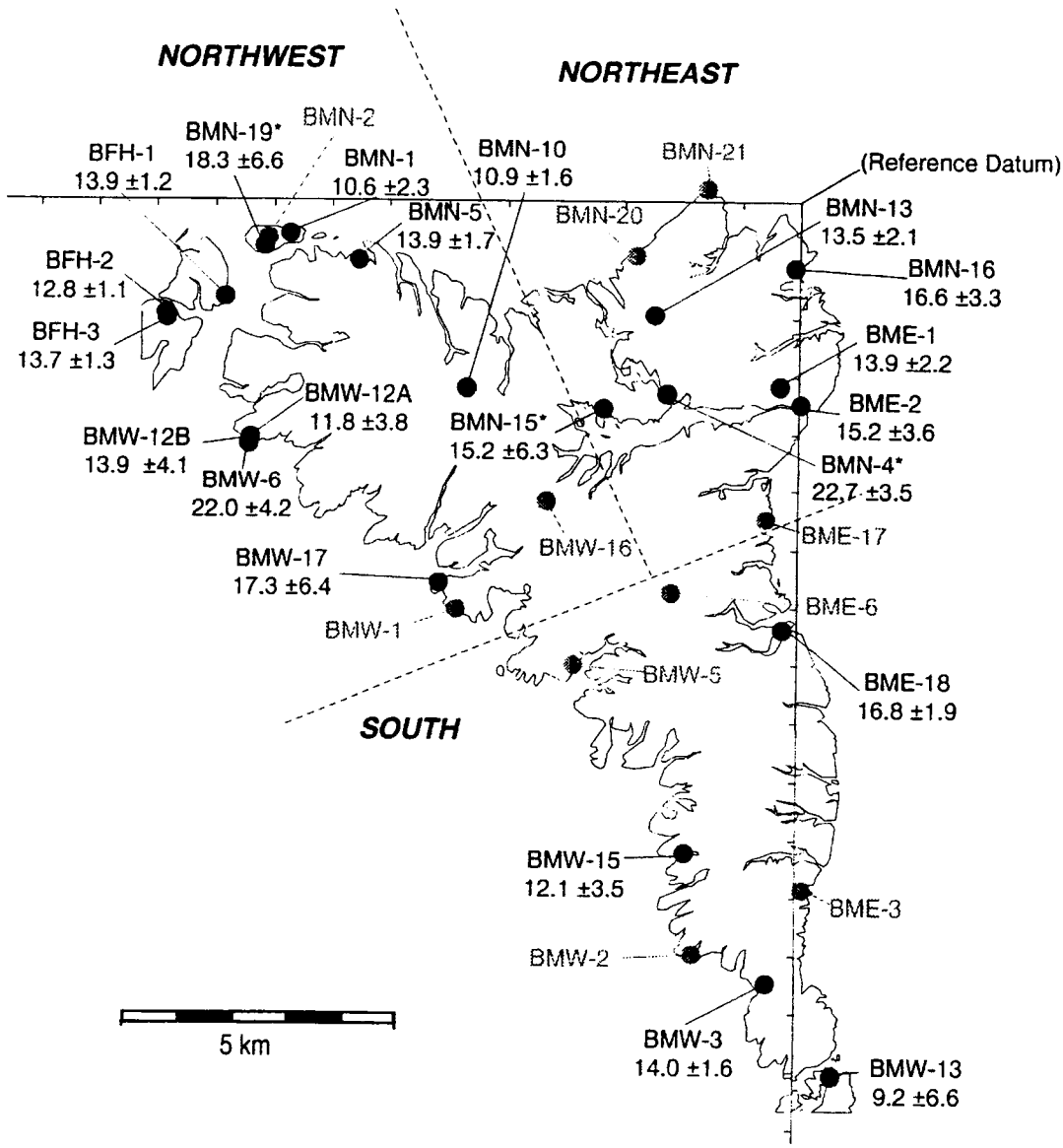

Stamatakos et al., Figure 3.

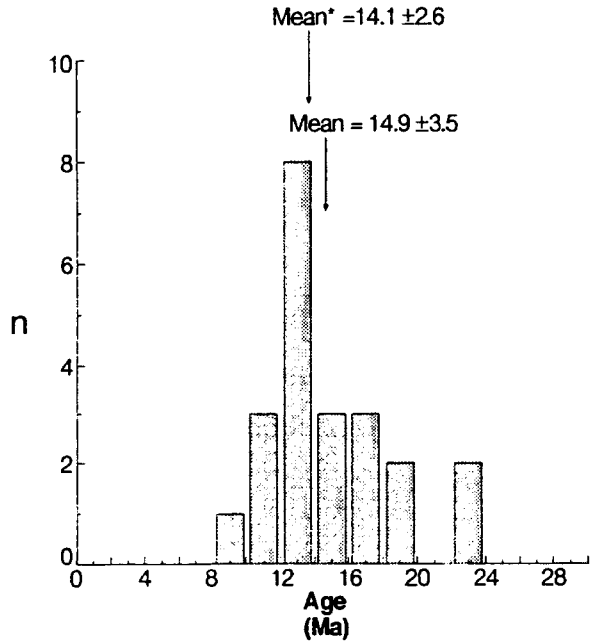

Stamatakos et al., Figure 4.

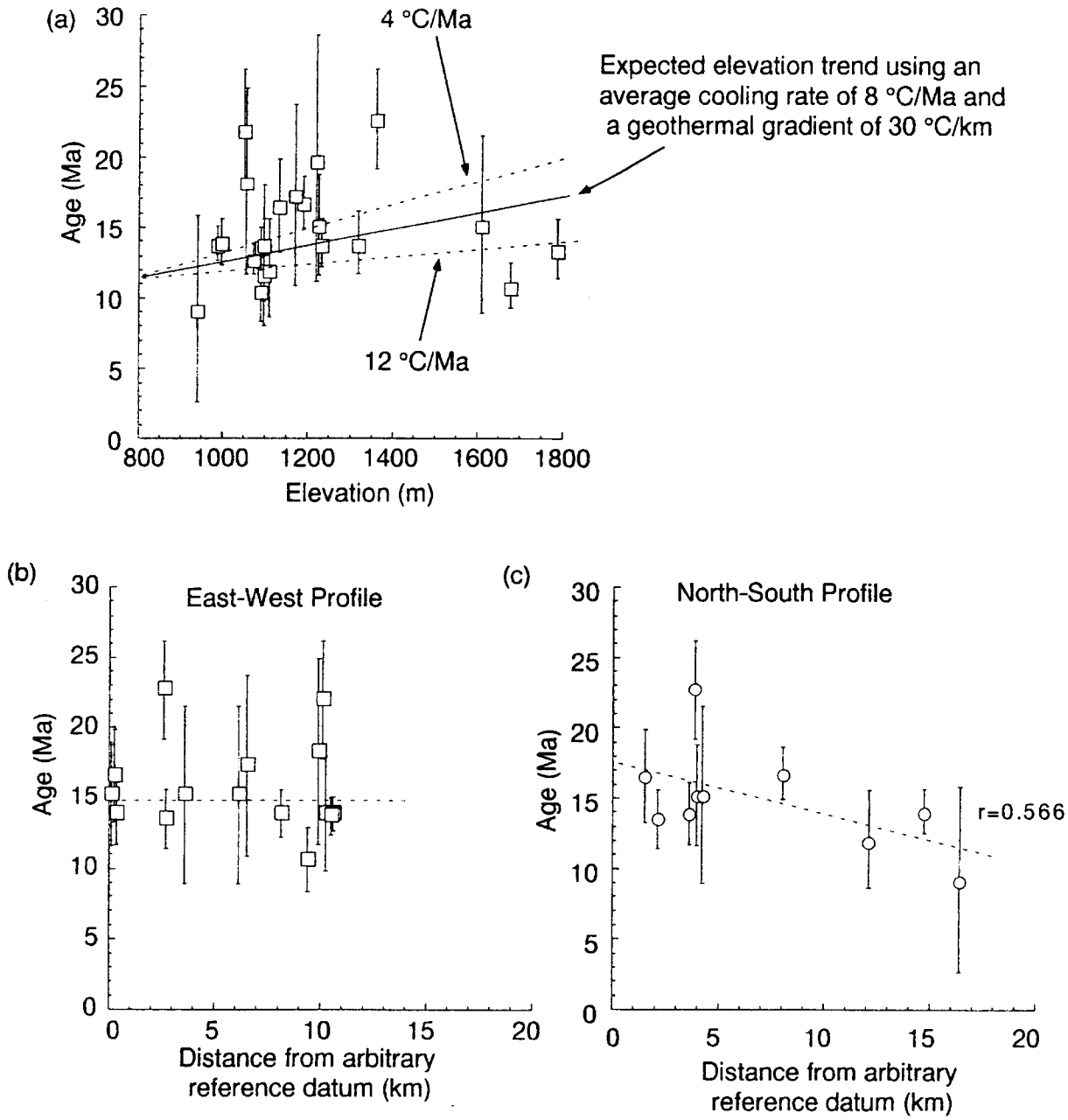

Stamatakos et al., Figure 5.

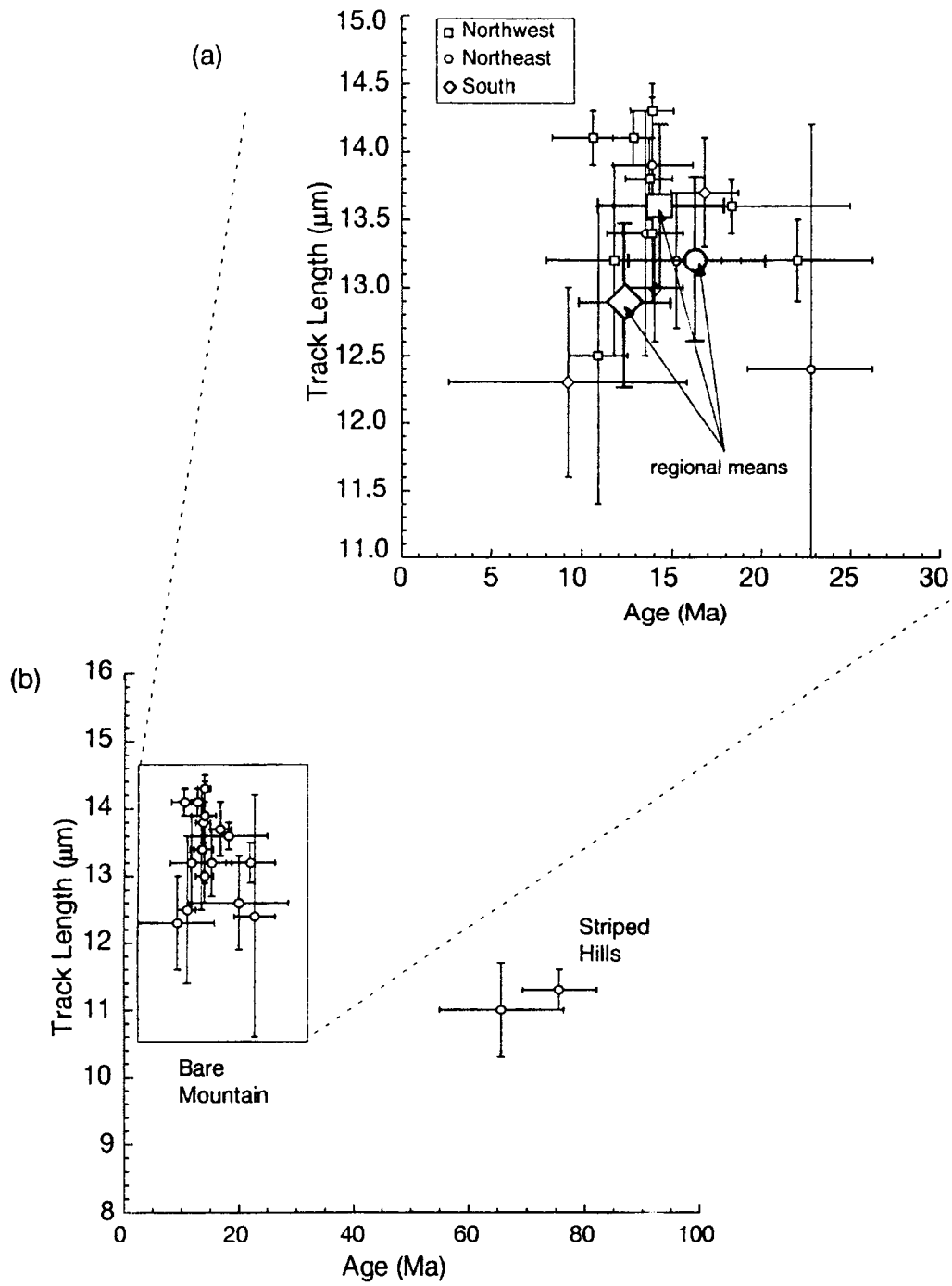

Stamatakos et al., Figure 6.

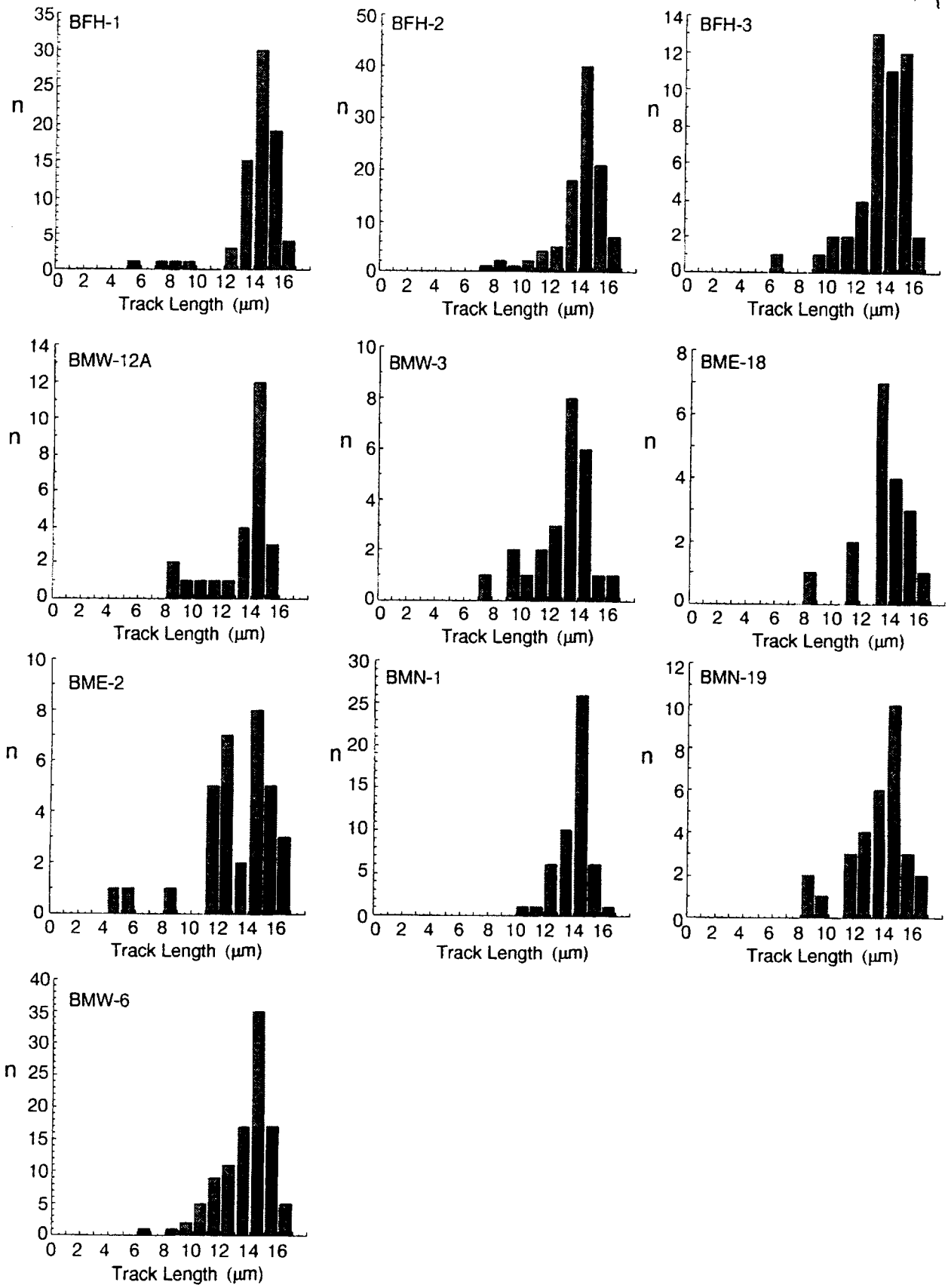

Stamatakos et al., Figure 7.

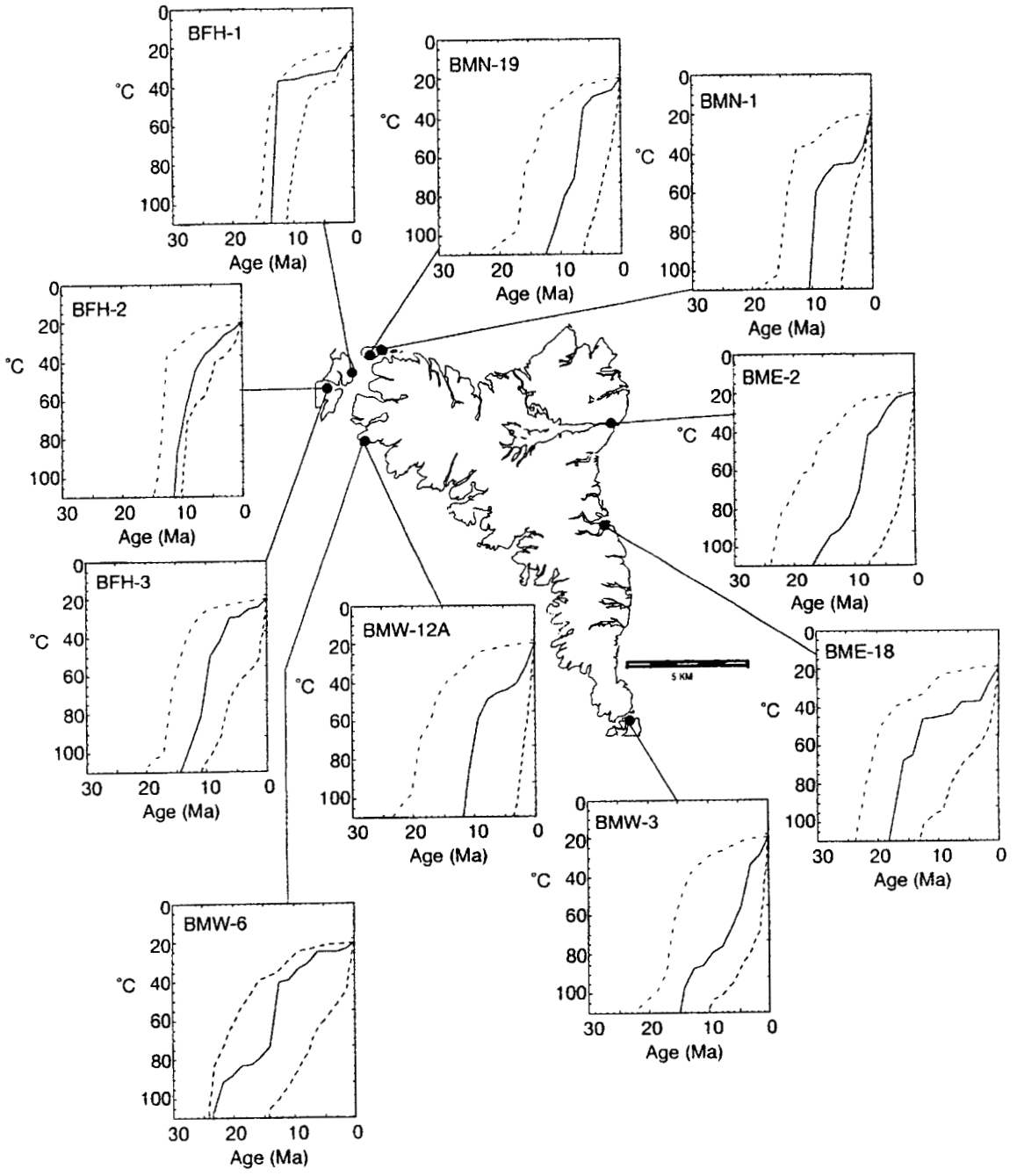

Stamatakos et al., Figure 8.

Composite Temperature-Time Curves

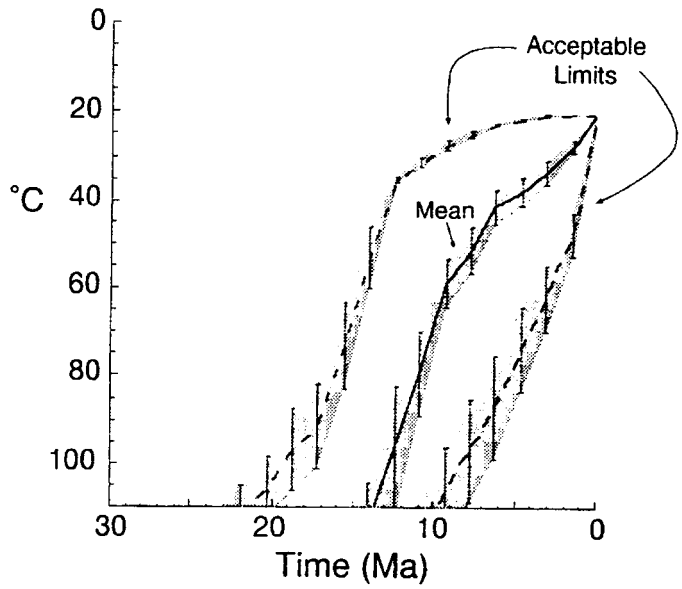

Stamatakos et al., Figure 9.

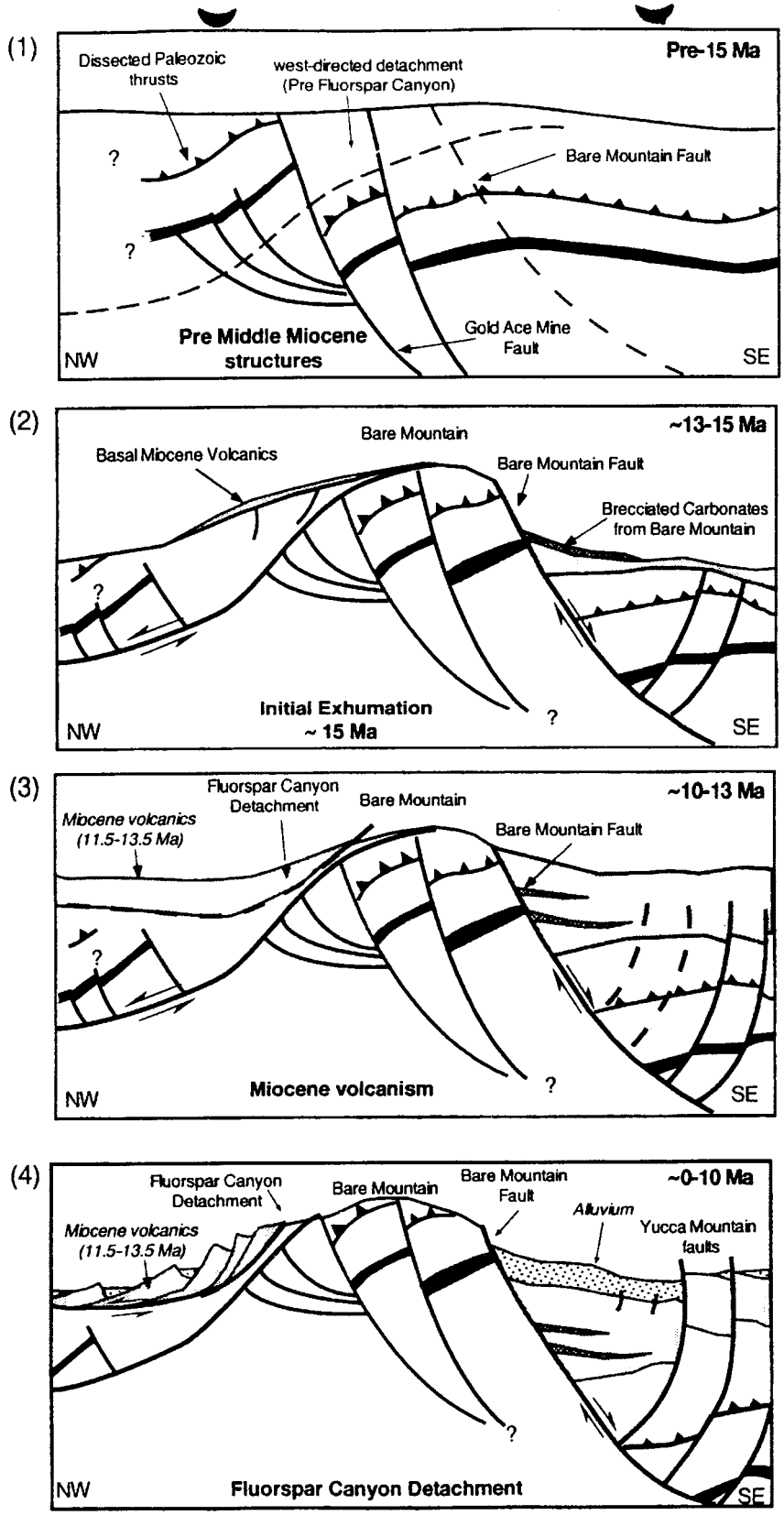

Stamatakos et al., Figure 10.